Semiconductor Physics, Quantum Electronics & Optoelectronics, 2012. V. 15, N 2. P. 170-175.

PACS 72.40.+w, 77.65.Ly, 81.05.Dz

Residual stresses and piezoelectric properties of the HgCdTe – based compound heterostructures under the anisotropic deformation restriction

A. B. Smirnov
V. Lashkaryov Institute of Semiconductor Physics of NAS of Ukraine
41, prospect Nauky, 03028 Kyev, Ukraine
Phone: (044) 525-18-13; fax: (044) 525 1810
E-mail: alex_tenet@isp.kiev.ua

Abstract. Narrow-gap mercury cadmium telluride thin films grown by MBE methods onto various substrates (HgCdTe/Si, HgCdTe/GaAs) were investigated as a piezoelectric heterostructure for IR detection. Mechanical stresses at the layer-substrate interface were analyzed. It was determined that for [310] oriented MCT-based structures under the anisotropic restriction of the deformation the nonzero shear components of the strain tensor arise and stress induced piezoelectric polarization is generated. Existence of the built-in electric field in the strained MCT-based heterostructure results in the spatial separation of the nonequilibrium carriers and the possibility of the room temperature detection of the IR radiation is realized.

Keywords: strained heterostructure, piezoelectric properties, HgCdTe.

Manuscript received 05.03.12; revised version received 20.03.12; accepted for publication 27.03.12; published online 15.05.12.

1. Introduction

Lattice strain is a matter of paramount importance for solid-state devices, and it is exploited to improve the electrical and optical properties of these devices. For example, significant enhancement in the hole mobility of a SiGe-on-insulator metal-oxide-semiconductor field-effect transistor was achieved using the lateral-strain-relaxation process [1].

An important phenomenon in strained structures grown along a polar crystallographic axis is availability of a piezoelectric field, which deeply modifies semiconductor band configuration and physical properties. Piezoelectric field in strained heterostructures was theoretically predicted in [2, 3] and then experimentally proved [4-6]. The fields in exceeding of 10^5 V/cm experimentally studied in III-V [7] and II-VI [8-10] heterostructures, can have applications in electro-optics and nonlinear optics [11, 12]. These electric fields can also cause charge accumulation, which can be used in a field effect transistor [13] and resonant tunneling structures. Strain-induced piezoelectric effects in arbitrary shaped II-VI quantum wires are described [14].

In this work, the HgCdTe (MCT) – based strained heterostructures are considered under the anisotropic restriction of the deformation. The purpose of this study is demonstration of the possibility to detect IR radiation by using piezoelectric heterostructure HgCdTe on Si without cryogenic cooling and to achieve its improved performance.

In this work, the following glassy system was investigated: As – S undoped and doped with manganese and chromium in various concentrations.

2. Experimental: MCT-based heterostructure growth and characterisation

The MCT-based heterostructure, shown in Fig. 1, was grown by MBE with intermediate buffer layers on [310]-oriented Si and GaAs substrates [15]. To decrease the influence of surface recombination, MCT layers were grown with the Cd content increasing to the surface.

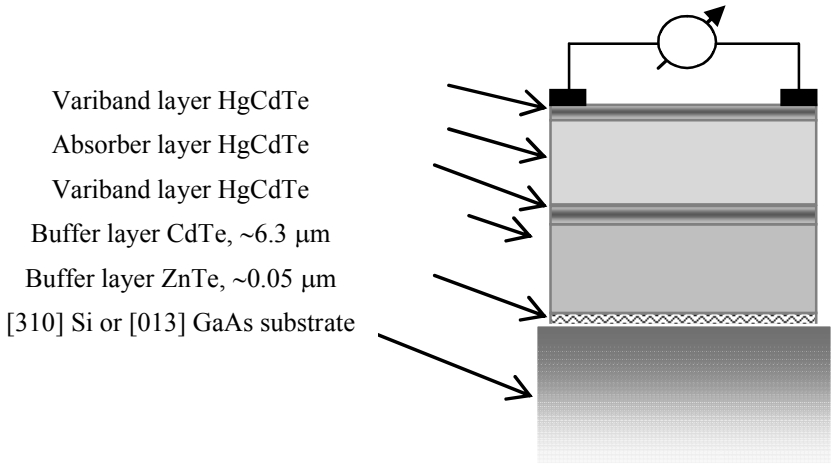

Fig. 1. A cross-sectional view of the typical MBE grown HgCdTe-based heterostructure with photolithographicaly patterned contact metallization.

Close to the buffer layer, the Cd content also increases, and a potential barrier can be formed in some cases between the buffer and photosensitive layers. The structures were characterized by X-ray diffraction, FTIR spectroscopy and temperature dependent Hall measurements. The change in the curvature radius (ΔR), measured by the changes of Bragg maximum angle position, before and after layer structure deposition, was used to estimate the residual stresses in the MCT-based heterostructures. Hall measurements allowed estimating the parameters of charge carrier transport (p~10^{16} cm^{-3}, μ_p~230 cm^{2}V^{-1}c^{-1} at 80 K). FTIR transmission analysis was used to determine the MCT composition.

3. Results and discussion

3.1. Residual stresses of the MCT – based heterostructures

It is worth noting that, for compound heterostructures (such as HgCdTe/CdTe/ZnTe/Si or HgCdTe/CdTe/ZnTe/GaAs, observable here), the presence of residual stresses is a specific character caused by their physical nature. Mechanical stresses arise from various causes, including the physical nature of the as-deposited material, thermal expansion difference between the film and substrate materials, chemical or structural changes occurring in the film in the course of processing.

The main factors determining the degree of perfection of the layer (l) - substrate (s) structure are the differences between their crystal lattice parameters $\Delta a = a_s - a_l$ and linear thermal expansion coefficients $\Delta\alpha = \alpha_s - \alpha_l$. The stress at the layer – substrate interface with a large difference between the lattice parameters can be expressed in the form [16]:

$$\sigma_{misfit} = \frac{E\varepsilon}{(1-\nu)}, \qquad (1)$$

where $\varepsilon = \Delta a / a_s$, E – is the Young modulus, ν - is the Poisson's ratio. For E and ν, the average values between the film and substrate are calculated. Calculations show that the initial misfit stress for all epitaxial systems under study is very large (~10^{10} Pa).

Achievements in crystal growth technology have improved the situation with heterostructures, which acquire strain owing to lattice mismatch. The well-known method of reducing mechanical stresses in a semiconductor heterostructure is based on use fitting to the lattice parameter of intermediate layers. During the growth process, the stresses decrease owing to the introduction of misfit dislocations, since the film thickness d increases and completely relaxes at a certain critical depth d_{cr}. A thickness-dependent misfit strain can be described as [17]:

$$\varepsilon(d) = \frac{d_{cr}}{d}\varepsilon_{init}, \qquad (2)$$

The critical thickness of CdTe on silicon was estimated to be approximately 0.5 nm and for CdTe on GaAs ~0.9 nm [17]. If the ZnTe nucleation layers are used, the critical thickness becomes equal to 1.2 nm in the case of Si substrate and 4 nm in the case of GaAs substrate [17]. For a CdTe film with the thickness close to 6.3 μm, which is typical for the film thicknesses used in this work, the thickness-dependent residual misfit stress calculated with regard to the equations (1) and (2) is σ^*_{misfit} equal to 6 MPa.

This value is significantly lower than the stress resulted from the thermal expansion mismatch:

$$\sigma_{thermal} = \frac{\Delta\alpha\Delta T E_l}{(1-\nu_l)}, \qquad (3)$$

where ΔT is the difference between the synthesis and operation temperatures. The absolute values of the thermal stresses for epitaxial systems under study reach ~10^7 Pa and they are quite similar to the data of ref. [17].

The residual stresses for heterostructures observable here were estimated experimentally by the X-ray diffraction technique. Due to strain-induced bowing, Bragg peak positions will differ slightly in different points on the film surface. X-ray diffraction rocking curve of full-width at half-maximum mapping is used to generate a surface profile from which a radius of curvature (ΔR) is extracted. The change in radius, before and after layer structure deposition, may be used to estimate the residual film stresses using the Shoney's equation:

$$\sigma_{\exp} = \frac{E_s d_s^2}{6(1-\nu_s) d_l} \frac{1}{\Delta R} \tag{4}$$

where d_l and d_s are the layer and substrate thicknesses, respectively, E_s and ν_s are the linear elastic modulus and Poisson′s ratio of the substrate respectively.

Calculated misfit and residual thermal stresses, obtained according to equations (1) – (3), as well as the absolute value of the experimentally determined residual stresses for heterostructures under study, reaches 2 to 15 MPa and are in agreement with the predicted data (see Table 1). The ZnTe layer was ignored during our stress analysis, since there is a presumption that the thick CdTe layer should dominate over the stress characteristics of the buffered substrate.

Table 1. Calculated (σ_{total}) and experimentally obtained (σ_{exp}) residual stresses for HgCdTe-based heterostructure, σ^*_{misfit} is a thickness-dependent misfit stress, $\sigma_{total} = \sigma^*_{misfit} + \sigma_{thermal}$.

Substrate	σ_{misfit}	σ^*_{misfit}	$\sigma_{thermal}$	σ_{total}	σ_{exp}
CdTe/ZnTe/GaAs	~-13 GPa	-8.6 MPa	-17 MPa	-25.6 MPa	~-2 MPa
CdTe/ZnTe/Si	~27 GPa	-5 MPa	50 MPa	45 MPa	~15 MPa

Thus, we have demonstrated the presence of residual stresses in the MCT-based heterostructures. In particular, CdTe/ZnTe/GaAs structure is grown in compression since the sign of σ_{total} (as well as σ_{exp}) is negative, whereas, for CdTe/ZnTe/Si structure, the total residual stresses are tensile.

Let us consider the mechanical deformations of a strained layer in the heterostructure with lattice mismatch in terms of local strains along the coordinate axes.

The standard strain – displacement ratio is given by below:

$$\varepsilon_{ij} = \frac{1}{2}\left(\frac{\partial u_i}{\partial x_j} + \frac{\partial u_j}{\partial x_i}\right) \tag{5}$$

where u_i and x_i denote displacement and space coordinate along the i-th crystallographic axis, respectively. For zinc-blend biaxial strained material grown on (001) surface the deformation components are derived as [18]:

$$\begin{aligned} &\varepsilon_{ij} = 0 (i \neq j), \\ &\varepsilon_{11} = \varepsilon_{22} = \varepsilon_{//}, \\ &\varepsilon_{33} = \varepsilon_{\perp} \end{aligned} \tag{6}$$

where the symbols || and ⊥ denote the xy-plane and the z-axis, respectively. The MCT-based heterostructure under study were grown in (310) orientation, and the principal coordinate system x-y-z does not coincide with that of the MCT unit cell. Tensors in the x-y-z coordinate system can be transformed to the MCT coordinate system x'-y'-z' using Euler's angles α, β, γ. The components of the strain in the new coordinate system are related by the equality $\varepsilon''_{ij} = c_{im} c_{jn} \varepsilon_{mn}$. The values of Euler's angles, as well as transformation matrix and strain tensor in the new coordinate systems for [310] and [111] directions are presented in Table 2.

The data in Table 2 clearly show that, for zinc-blend material grown on (001) surface substrate, only the stretching (compressive) strain components have nonzero values. At the same time, for the structure grown on (310) surface y-component of the shear strain acting on a plane perpendicular to the x-axis (ε_{xy}) as well as x-component of the shear strain acting on a plane perpendicular to the y-axis (ε_{yx}) have nonzero value. And, for the structure grown on (111) surface all strain components have nonzero values.

3.2. Piezoelectric properties of the MCT – based heterostructures

Under normal conditions, MCT crystallizes in F43m lattice (Td) and has one independent piezoelectric constant e_{14}. Therefore, mechanical stresses can induce electric fields and/or surface charges in MCT due to piezoelectric effects [8].

The piezoelectric effect can be described by the following equation:

$$P_i = e_{ijk} \varepsilon_{jk} = d_{ijk} \sigma_{jk} \tag{7}$$

where $\boldsymbol{P}_i$ are the polarization vectors, $\boldsymbol{\varepsilon}_{jk}$ and $\boldsymbol{\sigma}_{jk}$ are tensors of the mechanical strains and stresses, respectively, and $\boldsymbol{e}_{ijk}$ and $\boldsymbol{d}_{ijk}$ are the piezoelectric tensors.

For cubic symmetry, in principal coordinate axes, all the nonzero components of the piezoelectric tensor for F43m lattice are equal: $e_{123} = e_{132} = e_{231} = e_{213} = e_{312} = e_{321} = e_{14}$, where $e_{14} = 0.0136$ C/m^2 for MCT [9]. The matrix form of strain tensor is:

$$\begin{pmatrix} \varepsilon_{11} & \varepsilon_{12} & \varepsilon_{13} \\ \varepsilon_{21} & \varepsilon_{22} & \varepsilon_{23} \\ \varepsilon_{31} & \varepsilon_{32} & \varepsilon_{33} \end{pmatrix} = \begin{pmatrix} \varepsilon_1 & \frac{1}{2}\varepsilon_6 & \frac{1}{2}\varepsilon_5 \\ \frac{1}{2}\varepsilon_6 & \varepsilon_2 & \frac{1}{2}\varepsilon_4 \\ \frac{1}{2}\varepsilon_5 & \frac{1}{2}\varepsilon_4 & \varepsilon_3 \end{pmatrix} = \begin{pmatrix} \varepsilon_1 \\ \varepsilon_2 \\ \varepsilon_3 \\ \varepsilon_4 \\ \varepsilon_5 \\ \varepsilon_6 \end{pmatrix}, \tag{8}$$

Table 2. Strain transformation parameters for MCT-based heterostructures grown with (001), (310) and (111) orientation.

	The Euler's angles	Transformation matrix	Strain tensor in the new coordinate systems
OZ′||(001)	———	———	$\varepsilon'_{ij} = \begin{pmatrix} \varepsilon_{//} & 0 & 0 \\ 0 & \varepsilon_{//} & 0 \\ 0 & 0 & \varepsilon_{\perp} \end{pmatrix}$, $\varepsilon_{\perp} = -\frac{2c_{12}}{c_{11}}\varepsilon_{//}$
OZ′||(310)	α = -18.45°, β = -90°, γ = 0°	$C_{ij} = \begin{pmatrix} 0 & \sin\varphi & -\cos\varphi \\ 0 & \cos\varphi & \sin\varphi \\ 1 & 0 & 0 \end{pmatrix}$, $\varphi = -\alpha$	$\varepsilon'_{ij} = \begin{pmatrix} 0.1\varepsilon_{//} + 0.9\varepsilon_{\perp} & 0.3(\varepsilon_{//} - \varepsilon_{\perp}) & 0 \\ 0.3(\varepsilon_{//} - \varepsilon_{\perp}) & 0.1\varepsilon_{//} + 0.9\varepsilon_{\perp} & 0 \\ 0 & 0 & \varepsilon_{//} \end{pmatrix}$
OZ′||(111)	α = -45°, β = -54,73°, γ = 0°	$C_{ij} = \begin{pmatrix} \cos\varphi\cos\theta & -\sin\varphi & \cos\varphi\sin\theta \\ \sin\varphi\cos\theta & \cos\varphi & \sin\varphi\sin\theta \\ -\sin\theta & 0 & \cos\theta \end{pmatrix}$, $\varphi = -\alpha$, $\theta = -\beta$	$\varepsilon'_{ij} = \frac{1}{3}\begin{pmatrix} (2\varepsilon_{//} + \varepsilon_{\perp}) & (\varepsilon_{//} - \varepsilon_{\perp}) & (\varepsilon_{//} - \varepsilon_{\perp}) \\ (\varepsilon_{//} - \varepsilon_{\perp}) & (2\varepsilon_{//} + \varepsilon_{\perp}) & (\varepsilon_{\perp} - \varepsilon_{//}) \\ (\varepsilon_{//} - \varepsilon_{\perp}) & (\varepsilon_{\perp} - \varepsilon_{//}) & (2\varepsilon_{//} + \varepsilon_{\perp}) \end{pmatrix}$

and the matrix form of the induced polarization vector can be expressed as:

$$\begin{pmatrix} P_1 \\ P_2 \\ P_3 \end{pmatrix} = \begin{pmatrix} 0 & 0 & 0 & e_{14} & 0 & 0 \\ 0 & 0 & 0 & 0 & e_{14} & 0 \\ 0 & 0 & 0 & 0 & 0 & e_{14} \end{pmatrix} \begin{pmatrix} \varepsilon_1 \\ \varepsilon_2 \\ \varepsilon_3 \\ \varepsilon_4 \\ \varepsilon_5 \\ \varepsilon_6 \end{pmatrix} \quad (9)$$

It is necessary to note that only the shear strains can induce electric polarization, and the extensional strains do not induce polarization. It is easy to show that for zinc-blend biaxial strained bulk material, as well as for [100], [010], or [001]-oriented layer structures, the piezoresponse does not arise $P_i = e_{ijk}\varepsilon_{jk} = 0$.

But for the anisotropic restriction of the deformation, when the substrate specifies the strain of layer along the x and y axes, the values of ε_{11} and ε_{22} are specified by a thickness-dependent misfit as well as a thermal expansion mismatch strain in *xy*-plane (see eq.1-3) and they are different from the value of ε_{33} (see eq.6).Consequently, nonzero shear strain components appear as a result of strain tensor transformation (see Table 2).

The components of the piezoelectric tensor in the new coordinate system are related by the equality $e''_{ijk} = c_{im}c_{jn}c_{kl}e_{mnl}$ and for [310]-oriented MCT layer in the new coordinate system the induced polarization vector is derived as:

$$\begin{pmatrix} P_1 \\ P_2 \\ P_3 \end{pmatrix} = 0.6e_{14}\cos 2\varphi \begin{pmatrix} 0 \\ 0 \\ \varepsilon_{//} - \varepsilon_{\perp} \end{pmatrix} \quad (10)$$

Like to that for the [111]-oriented MCT layer the induced polarization vector is derived as:

$$\begin{pmatrix} P_1 \\ P_2 \\ P_3 \end{pmatrix} = \frac{2}{3}e_{14}\begin{pmatrix} \varepsilon_{\perp} - \varepsilon_{//} \\ \varepsilon_{//} - \varepsilon_{\perp} \\ \varepsilon_{//} - \varepsilon_{\perp} \end{pmatrix} \quad (11)$$

It is worth noting that, for [100], [010], or [001]-oriented MCT layers, no piezoelectric polarization will be induced.

Thus, for [310] oriented MCT-based structures with the anisotropic deformation restriction the nonzero shear strain components arise. As a consequence, electric polarization is generated in a strained heterostructure (see Eq.10). On the base of the experimentally obtained residual stresses for the MCT-based heterostructures, the value of the plane strain is estimated to reach $1.3\text{x}10^{-4}$ for MCT on Si structure and $0.17\text{x}10^{-4}$ for MCT on GaAs structure. The values of the induced polarization P_3 of the [310]-oriented MCT layer grown onto various substrates are found to be in the range from $0.85\text{x}10^{-6}$ C m^{-2} (MCT/Si) down to $0.1\text{x}10^{-6}$ C m^{-2} (MCT/GaAs), and, the electric field is found to be in the range from 0.6 kV m^{-1} (MCT/GaAs) to 5 kV m^{-1} (MCT/Si) estimated according to equations $\boldsymbol{E}_3 = \boldsymbol{-P}_3 / \varepsilon \cdot \varepsilon_0$.

Evidently, it is need to take into account that variband layer at the MCT surface also creates built-in

electric field in the heterostructure: $E_{variband} = \frac{1}{e}\frac{dE_g}{dx}$. This field tends to push carriers into the sample and an excess of the negative charge is accumulated on the surface of the sample with *p*-type conductivity. Consequently, the variband built-in electric field is directed to the structure surface in the same direction as the piezoelectric field induced by tensile stresses (MCT/Si). The resultant built-in electric field value will be reinforced. At the same time, the piezoelectric field induced by compressive stresses in MCT/GaAs heterostructure is directed into the sample. It is opposite to the direction of the variband built-in electric field, and the resultant field can be canceled.

3.3. Room temperature IR detection

It is well known that thermal processes dominate at temperatures close to the room one in MCT-based devices used for middle and long wavelength IR spectral regions, and in the conventional photon detector it is impossible to accurately detect any infrared radiation other than that of high output power as in a CO_2 gas laser. Conventional MCT-based photon detectors need significant cooling in order to reduce noise and leakage currents resulting from generation and recombination processes.

It has been recently suggested that Auger recombination and generation rates can be reduced using the phenomena of exclusion and extraction to produce nonequilibrium carrier distributions [19]. Photodiode HgCdTe/Si structures based on this concept were manufactured for near-room temperature operation. In addition, three types of IR photovoltaic detectors can operate at near-room temperature: photoelectromagnetic detectors, magnetoconcentration detectors, and Dember effect detectors [20]. The operation principle of these devices is based on the separation of excess carriers.

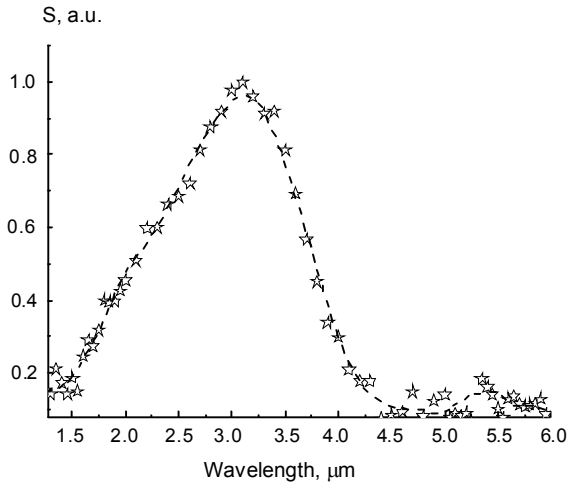

Fig. 2. Spectra of the photovoltaic responsitivity of the $Hg_{0.7}Cd_{0.3}Te$/Si element.

Existence of the built-in electric field in the studied herein strained MCT-based heterostructures results in the spatial separation of the nonequilibrium carriers, too. As a consequence, the possibility of the room temperature detection of the IR radiation is implemented. In particular, for MCT/Si stressed semiconductor heterostructure with piezoelectric properties. At the same time, the built-in electric field in MCT/GaAs heterostructure is very likely compensated, and we cannot detect IR radiation at room temperature.

This conclusion was confirmed experimentally elsewhere [21, 22]. It was observed that $Hg_{0.68}Cd_{0.32}Te$/CdTe/ZnTe/Si heterostructure obtained by MBE method exhibits spectral photoresponse under IR photoexcitation without electrical bias at room temperature (see Fig. 2). At the same time, spectral response of the MCT-based structures grown on GaAs substrates was insignificant.

To estimate the voltage responsivity, the prototype of MCT-based photovoltaic detector was exposed to infrared photons from a laser source (continuously operating He-Ne laser, LGN 113) with the wavelengths 0.63, 1.15 and 3.39 μm. The measured value of responsivity was from ~0.5 V/W to ~4.3 V/W at 0.5 mW laser beam power in the focal spot [21]. It was also found out that the prototype of photovoltaic detector is sensitive to CO_2 laser radiation on the level of ~0.04 V/W at 1 mW laser beam power in the focal spot [22]. An element of the prototype (1x1 mm) achieves photovoltaic spectral sensitivity at the level $D^* = 2.6 \cdot 10^9$ ($W^{-1}cm\ Hz^{1/2}$) for 300 K and λ~3 μm. The noise measurements were performed with the 1 Hz bandwidth.

4. Conclusions

Thus, the presence of residual stresses in HgCdTe-based heterostructures grown by MBE with intermediate buffer layers on [310]-oriented Si and GaAs substrates was demonstrated. In particular, HgCdTe/CdTe/ZnTe/GaAs structure was grown in compression stresses, whereas, for HgCdTe/CdTe/ZnTe/Si structure, the total residual stresses are tensile. It was obtained that the experimentally confirmed stress for heterostructures under the study reaches 2 to 15 MPa and is in agreement with the predicted data.

It was confirmed that for [310] oriented MCT-based structures under the anisotropic restriction of deformation, when the substrate specifies the in-plane strain of layer, the nonzero shear components of the strain tensor arise and stress induced piezoelectric polarization is generated. Existence of the built-in electric field in the studied herein strained MCT-based heterostructures observable here results in the spatial separation of the nonequilibrium carriers and the possibility of the room temperature detection of the IR radiation is realized. This conclusion is confirmed experimentally.

Acknowledgment

The authors would like to express their thanks Dr R Savkina all her critical help in the process writing this article.

References

1. T. Irisawa, T. Numata, T. Tezuka, K. Usuda, N. Hirashita, N. Sugiyama, E. Toyoda, and S. Takagi, High Performance Uniaxially Strained SGOI pMOSFETs Fabricated by Lateral Strain Relaxation Technique on Globally Strained SGOI// *IEEE Trans. Electron Devices* **53**, p. 2809-2815 (2006).
2. D.L. Smith, Strain-generated electric fields in [111] growth axis strained-layer superlattices // *Solid State Commun*. **57**, p. 919-921 (1986).
3. D.L. Smith and C. Mailhiot, Theory of semiconductor superlattice electronic structure// *Rev. Mod. Phys*. **62**, p. 173-234 (1990).
4. B.K. Laurich, K. Elcess, C.G. Fonstad, J.G.Beery, C. Mailhot and D.L. Smith, Optical Properties of (100) - and (111)-Oriented GaInAs/GaAs Strained-Layer Superlattices // *Phys. Rev. Lett.* **62** p. 649 (1989).
5. I. Sela, D.E. Watkins, B.K. Laurich, D.L. Smith, S. Subbanna and H. Kroemer, Excitonic optical nonlinearity induced by internal field screening in (211) oriented strained-layer superlattices // *Appl. Phys. Lett.* **58** p. 684 (1991).
6. K. W. Goossen, E.A. Caridi, T.Y. Chang, J.B. Stark, D.A.B. Miller, and R.A. Morgan, Observation of room-temperature blue shift and bistability in a strained InGaAs-GaAs 〈111〉 self-electro-optic effect device Direct demonstration of a misfit strain-generated electric field in a [111] growth axis zinc-blende heterostructure // *Appl. Phys. Lett.* **56** p. 715 (1990).
7. E. A. Caridi, T. Y. Chang, K. W. Goossen and L. Eastman, Direct demonstration of a misfit strain-generated electric field in a [111] growth axis zinc-blende heterostructure //*Appl. Phys. Lett.* **56** p. 659 (1990).
8. C. F. Wan, J. D. Luttmer, R. S. List, and R. L. Strong, Piezoelectric effects in HgCdTe devices // *Journal of Electronic Materials* **24** p. 1293-1297 (1995).
9. A. T. Paxton, A. Sher, M. Berding, M. Van Schilfgaarde, and M. W. Muller, How dislocations affect transport //*Journal of Electronic Materials* **24** p. 525 (1995).
10. R. Andre, C. Deshayes, J. Cibert, L. S. Dang, S. Tatarenko and K. Saminadayar, Optical studies of the piezoelectric effect in (111)-oriented CdTe/ $Cd_{1-x}Zn_xTe$ strained quantum wells //*Phys. Rev. B* **42** p.11392-11395 (1990).
11. V. Ortiz, N. T. Pelekanos, and G. Mula, Efficient all-optical light modulation in a piezoelectric heterostructure at room temperature // *Appl. Phys. Letters* **72** p.963 (1998).
12. D.L. Smith, Piezoelectric effects in strained layer heterostructures grown on novel index // *Microelectronics Journal Volume* **28** p.707 (1997).
13. Peng Fei, Ping-Hung Yeh, Jun Zhou, Sheng Xu, Yifan Gao, Jinhui Song, Yudong Gu, Yanyi Huang, and Zhong Lin Wang, Piezoelectric Potential Gated Field-Effect Transistor Based on a Free-Standing ZnO Wire // *Nano Letters* **9** p.3435 (2009).
14. S. Patil, B. Wen and R. V. N. Melnik, Strain E□ects and Temperature-Dependent Phase Stability of II-VI Semiconductor Nanostructures // *AIP Conf. Proc*. **1199** p.303 (2010).
15. V. Yakushev, V. S. Varavin, V. V. Vasiliev, S. A. Dvoretsky, I. V. Sabinina, U. G. Sidorov, A. Sorochkin, and A. L. Aseev, *Photodiodes*, ed Jeong-Woo Park (InTech), (2011) p. 367-400.
16. Yu. L. Tkhorik and L. S. Khazan, *Plastic Deformation and Misfit Dislocations in Heteroepitaxial Systems* (Kiev: Naukova Dumka) [in Russian] (1983) p.304.
17. R.N. Jacobs, L.A. Almeida, J. Markunas, J. Pellegrino, M. Groenert, M. Jaime-Vasquez, N. Mahadik, C. Andrews, S. B. Qadri, T. Lee, and M. Kim //*Journal of Electronic Materials* **37** p. 1480 (2008).
18. K. Arimoto, and K. Nakagawa, Elastic theory for strained heterostructures with in-plane anisotropy //*J. Appl. Phys.* **104**, p. 063512-8 (2008).
19. T. Ashley, C. T. Elliott, and A. T. Harker, Non-equilibrium modes of operation for infrared detectors // *Infrared Phys.* **26**, p. 303-315 (1986).
20. J. Piotrowski and A. Rogalski, Uncooled long wavelength infrared photondetectors // *Infrared Physics Technology* **46**, p. 115-131 (2004).
21. T. Kryshtab, R. Savkina, F. Sizov, A. Smirnov, M. Kladkevich, and V. Samoylov, Infrared radiation detection by a piezoelectric heterostructure at room temperature // *Physica Status Solidi* (c) **9,** *in press* **(**2012).
22. F.F. Sizov, A.B. Smirnov, R.K. Savkina, V.A. Deriglazov, M.V. Yakushev, Narrow-gap piezoelectric heterostructure as IR detector // *Semiconductor physics, quantum electronics and photoelectronics* **15**, p. 65-71 (2012) (www.journal-spqeo.org.ua).